Dissociation of reliability, predictability, and heritability in fine- and coarse-scale functional connectomes during development

Erica L. Busch[1†], Kristina M. Rapuano[1], Kevin Anderson[1], Monica D. Rosenberg[2], Richard Watts[1], BJ Casey[1], James Haxby[3], Ma Feilong[3†]

[1]Department of Psychology, Yale University
[2]Department of Psychology, University of Chicago
[3]Department of Psychological and Brain Sciences, Dartmouth College

[†]Corresponding authors:
Erica L. Busch: Erica.Busch@yale.edu
Ma Feilong: feilong.ma@dartmouth.edu

Abstract

The functional connectome supports information transmission through the brain at various spatial scales, from exchange between broad cortical regions to finer-scale connections that underlie specific information processing mechanisms. In adults, while both the coarse- and fine-scale functional connectomes predict cognition, the fine-scale can predict twice the variance. Yet, past brain-wide association studies, particularly using large developmental samples, limit their focus to the coarse connectome to understand the neural underpinnings of individual differences in cognition. We examine resting-state fMRI (n=1,115 children, 389 twin pairs) and use hyperalignment to access reliable information in the fine-scale connectome. Though individual differences in the fine-scale connectome are more reliable than those in the coarse-scale, they are less heritable. Further, the alignment and scale of connectomes influence their ability to predict behavior: both scales equally predict more heritable cognitive traits, but the fine-scale connectome predicts less heritable traits significantly better than the coarse-scale.

Introduction

The building blocks of the functional connectome are an interplay of genetics[1–3] and experience[4,5]. Functional connections at various spatial scales, ranging from coarse, global regional oscillations to fine, vertex-wise patterns of information transfer, account for related yet distinct types of information encoding and transmission[6,7]. While variation in functional connectivity can predict individual differences in aspects of memory[8], attention[9], and intelligence[10], among other cognitive traits[10–15], it is unclear how the spatial scales of functional connectomes differentially relate to genetic and experience-based cognitive traits during periods of biological and experiential development. To understand how this is reflected at the population level in the developing brain requires consideration of how we define functional connectivity information at both fine and coarse scales. In the current study, we disentangle more experience-based attributes of the functional connectome from genetic influences by estimating the heritability, reliability, and predictive validity of resting-state functional connectivity (RSFC) during development[16,17] in twins and unrelated children at different levels of the granularity of connectome organization.

Past studies using structural and functional magnetic resonance imaging (MRI) of twin samples have revealed strong genetic control over various measures of brain morphology[4,18–21] and RSFC[2,3,22–26]. Genetic influences on brain structure and function are associated with cognitive functioning[18], increase with age[18,27], and interact with the environment to sculpt an individual's functional connectome[1,18,27,28]. RSFC is a powerful tool for investigating individual differences in brain–behavioral associations, especially in clinical and developmental populations where task-based fMRI is often difficult[11,13,14,29]. Of neuroimaging phenotypes, recent studies indicate

that structural MRI is more heritable than resting-state fMRI, which is in turn more heritable than task-based fMRI[19]. For this reason, we focus on resting-state functional connectivity (RSFC) to understand the nature of individual differences in the brain and behavior in childhood.

Prior work has established heritability of RSFC between specific regions of interest[30] and whole-brain oscillations between large cortical regions or networks[3,5,22,24,25]. In whole-brain studies, functional connectivity is commonly calculated by dividing the cortex into parcels and collapsing over the hundreds of vertices within a parcel, then correlating the average timeseries between each pair of parcels. This approach aims to mitigate high-dimensionality, measurement instabilities, and inter-individual differences in the brain's functional organization, and has been used in prior studies relating RSFC and cognition in development[11,15,31]. Within developmental samples, parcellations are believed to account for developmental differences in cortical anatomy by coarsely aligning fMRI signals across subjects. However, group parcellations are defined on average adult brains and assume that the same boundaries around brain regions exist in the same location across all brains, regardless of inter-subject or developmental differences[32]. Individual-defined parcellations better capture individualized functional topography[24,33–35], but still, typical parcels may cover a larger surface area than is most informative and effects that may be present for a subset of vertices in a parcel can be obscured by aggregating into a single parcel[32]. More generally, both types of parcellations collapse over local information processing at the fine-scale, which has been shown to reliably represent behaviorally-relevant information[12].

A useful alternative to group-average parcellations, functional alignment of fMRI data maximizes the intersubject correspondence of cortical information processing while resolving

variation in cortical anatomy at the fine-scale. Reliable, predictive individual differences in fine-scale signals are most apparent after resolving idiosyncrasies of individual functional topographies with methods like hyperalignment[6,36]. In this study, modeling the developing functional connectome at the fine-scale with hyperalignment allows two main affordances. First, functional alignment improves between-subject correspondence of both cortical responses and functional connectivity[36–40] and highlights reliable[41] and behaviorally-relevant[12] individual differences. Second, hyperalignment allows us to disentangle idiosyncratic anatomical topography from functional topography[6], and enables us to ask how individual differences in RSFC relate to genetics and behavior, independent of anatomical similarity.

Cortical architecture changes rapidly and idiosyncratically across development[42], which prompts important concerns about anatomical differences confounding our understanding of brain–behavior relationships in children. Accessing the cortex's fine-scale functional topography mitigates these concerns by retaining high dimensionality in a representational space disentangled from brain anatomy. To date, genetic contributions to the fine-scale functional connectome remain to be quantified, as well as their reliability and behavioral relevance during development. The current study seeks to address the following questions: Does accessing the fine-scale connectome tighten the link between functional connectivity, cognition, and genetics shown in the coarse-scale connectome? Or is there a dissociation of genetic control over these two scales of connectivity? Here, we use connectivity hyperalignment[38] to access and dissociate fine-scale and coarse-scale RSFC in a cohort of 1,115 9–10 year-olds from the Adolescent Brain Cognitive Development (ABCD) Study®[16] (Figure 1). We leverage machine learning approaches

to understand how connectome granularity relates to reliability, heritability, and neurocognitive abilities in children.

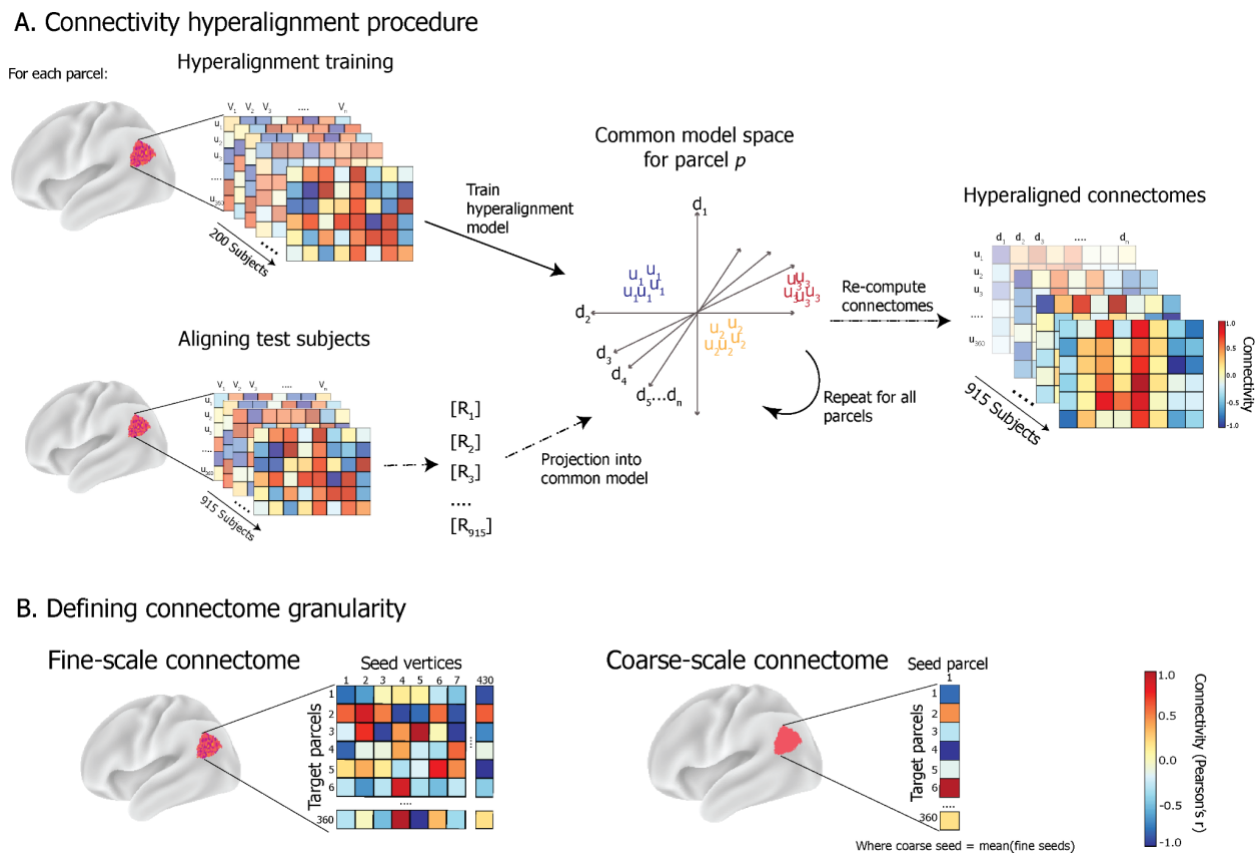

Figure 1: Methods

A. Connectivity hyperalignment training procedure. For each parcel in the Glasser parcellation (here, region 329 with 430 cortical vertices), connectivity matrices are computed as the strength of connectivity (Pearson's correlation) between the activity timeseries of vertices within the parcel (seeds; *u*) and the average activation across vertices in all other parcels (targets; *v*). The connectivity matrices for 200 held-out subjects are used to train the hyperalignment common model space for a given parcel. The model space is of dimensions **D** = [$d_1 \ldots d_n$] which are weighted combinations of **U** = [$u_1 \ldots u_n$], the dimensions of each subject's connectivity matrices in their native anatomical space. **D** represents the space where connectivity targets are

best aligned across training subjects. Then, connectomes for the 915 test subjects are projected into **D** via subject-specific transformation matrices **R**, which detail a mapping from given subject *i's* anatomical space $\mathbf{U_i}$ into **D.** This procedure is repeated to derive **R** for each test subject and parcel. Then, the regional activation pattern for each parcel in anatomical space is mapped via **R** into the region's common space to compute the hyperaligned timeseries for each subject, which is then used to recompute connectivity matrices between hyperaligned seeds *v* and model dimensions *d.* **B. Connectome granularity.** Fine-scale connectomes are multivariate patterns of the connectivity weights between the time-series responses of all individual vertices in a given parcel and the average time-series response of each other parcel in the brain. Coarse-scale connectomes are vectors (univariate), representing the connectivity weight between the average time-series response of a given parcel, averaged across all of its vertices, and those of each other parcel in the brain.

Results

Establishing the reliability of individual differences

Variability in RSFC can reflect idiosyncrasies driven by cortical communication patterns indicative of neurocognitive variability, but it can also reflect artifacts due to data acquisition noise, movement[43,44], and functional–anatomical mismatch. In adult populations, brain parcellations (e.g., Glasser parcellation[33]) average adjacent areas of cortex to improve signal-to-noise and reduce the dimensionality of the data, and adult-defined parcellations are frequently applied to development datasets[15,31]. This approach assumes functional–anatomical correspondence will improve at the group level and that functional boundaries are constant across development, and comes at the cost of lower granularity.

Here, we analyzed RSFC in a large cohort of 1,115 children, aged nine to ten, including 389 twin pairs (see Table S1 for subject breakdown) using two methods of group alignment. The first uses a standard approach to align data in a common space based on anatomical location (anatomical alignment [AA]), while the second approach uses connectivity hyperalignment (CHA)[38] to learn a common information space based on patterns of functional connectivity via an adapted Generalized Procrustes Analysis. CHA allows for local remixing of vertex-wise functional connectivity profiles (vertices' vectors of connectivity to targets) within an anatomically-constrained region[36], thereby projecting idiosyncratic patterns of vertex connectivities to the same target into a common template connectome[6]. In contrast with coarse alignment, which averages time-series responses across a region's vertices to calculate a single connectivity strength with each target region, CHA retains the vertex-by-vertex variation on connectivity strength to each target region (Figure 1B). Within this common, fine-grained space, individual differences in functional connectivity become more pronounced and reliable[41] and are more predictive of cognitive traits[12] in adults.

To address the question of individual differences in fine-scale functional connectivity among children, we present (to our knowledge) the first derivation of a child-defined and applied model of shared brain function, which negates concerns about differences in cortical development or anatomy that may confound modeling of functional connectivity patterns. To do this, we used CHA to build a template common connectome for each parcel on a training sample of 200 unrelated children, counterbalanced across included sites and representative of demographics within site (Table S1; Figures S1, S2, S3). We then hyperaligned each of the 915 remaining connectomes to this common connectome. Note that this common information space is based on

children of the same age and demographics as the test sample, and that the test sample's data played no role in deriving the common space. We addressed the relative effects of hyperalignment versus simply higher-dimensional measurements by averaging the functionally-aligned CHA data and by retaining the high-dimensional, anatomically aligned data, to have a full comparison of connectomes that are aligned anatomically, at both the coarse-grained and fine-grained level, and connectomes that are CHA-aligned, at both the coarse-grained and fine-grained level.

Since this is the first time a functional alignment algorithm has been trained and tested on a developmental cohort, we first established that idiosyncrasies in cortical activity patterns were, indeed, more reliable after fine-scale hyperalignment, as has been shown in adult cohorts[41]. We analyzed the reliability of idiosyncrasies in functional connectivity patterns across connectome alignment and granularity. Here, we define idiosyncrasies in terms of individual differences matrices (IDMs), or the pairwise correlation distance between all pairs of subjects. IDMs capture the dissimilarity structure (or idiosyncrasies) of functional connectivity patterns across subjects. We assessed the reliability of these idiosyncrasies by splitting each subject's RS timeseries in half to create two "pseudo-sessions" and calculating independent connectomes each split-half, then computing an IDM for each pseudo-session. We then correlated the two pseudo-sessions IDMs to measure the reliability of individual differences. This process was performed for anatomically-aligned coarse-grained and fine-grained connectomes and for CHA-aligned coarse-grained and fine-grained connectomes separately (see Individual differences matrix (IDM) reliability for more information).

CHA, particularly at the fine scale, improved the reliability of individual differences in functional connectivity over anatomical alignment alone (Figure 2). Across all parcels, reliability of coarse connectomes increased from an average of $r = 0.34 \pm 0.1$ for AA to $r = 0.58 \pm 0.08$ for CHA. Reliability of fine connectomes increased from an average of $r = 0.43 \pm 0.11$ for AA to $r = 0.86 \pm 0.07$ for CHA. After CHA, 100% of parcels at both scales showed greater reliability, and 99% of parcels showed greater reliability at the fine scale than the coarse scale. Notably, all four types of connectomes showed high split-half reliability, with CHA affording the greatest reliability. This result establishes that hyperalignment improves access to reliable information within an individual's functional connectome. Particularly at the fine scale, individual differences in functional connectivity were highly reliable, affording confidence in subsequent results based on these connectomes.

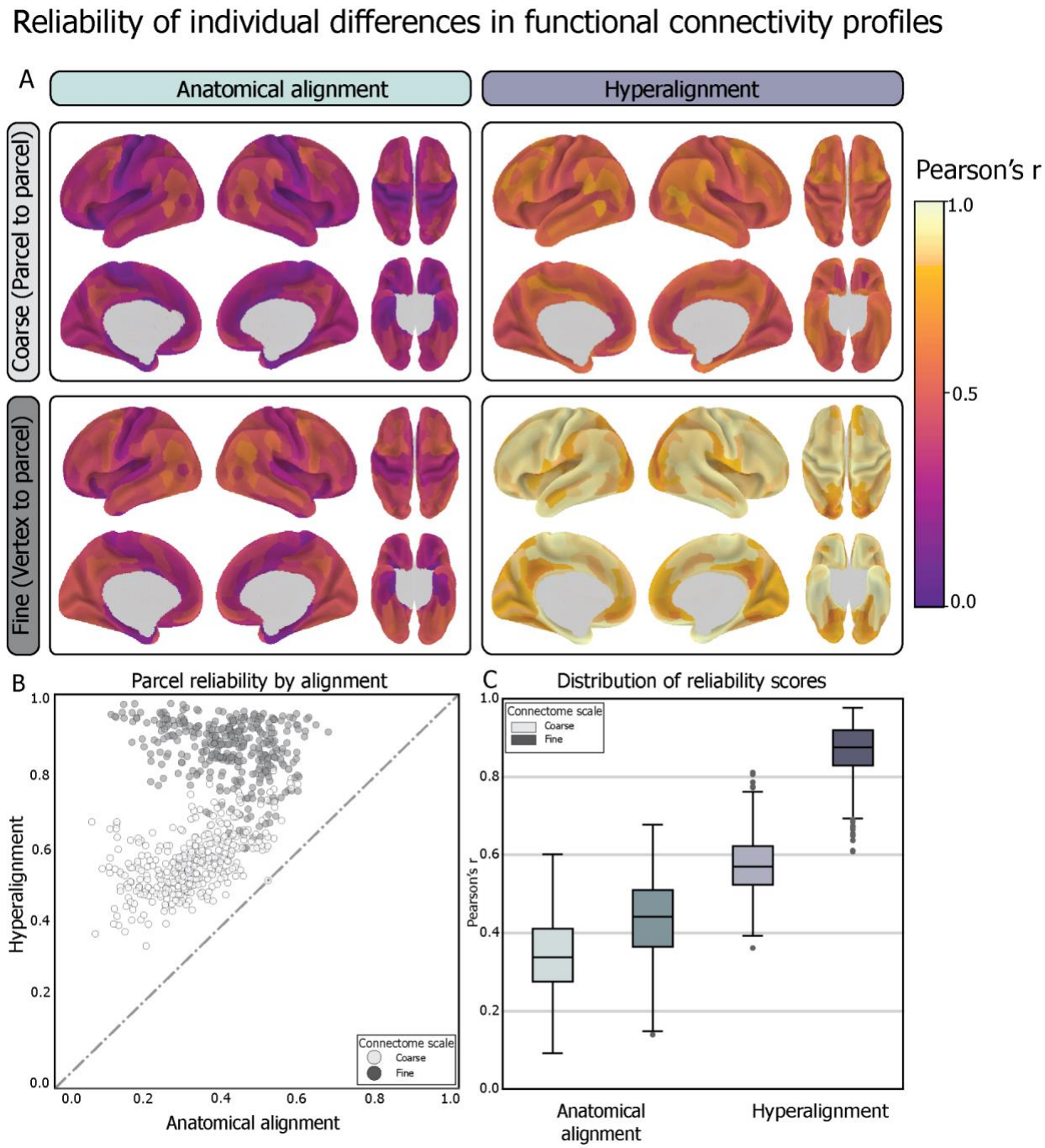

Figure 2. Reliability of individual differences in functional connectivity profiles

Procedure: The reliability of individual differences in functional connectivity profiles between regions (defined with the Glasser parcellation[33]) was analyzed with data from 526 unrelated

subjects. Subjects' timeseries data for each parcel were split into two halves, which were hyperaligned into the trained common space separately. For each region, split-half timeseries data pre- and post-hyperalignment were used to compute functional connectivity profiles at the fine and coarse scales. Then, individual differences matrices (IDMs) were computed across all pairs of subjects for each independent split half. The IDMs for each pair of split halves were then correlated (Pearson's r) for each region. Reliabilities of individual differences captured by regional functional connectivity profiles are presented on the cortex for the coarse and fine scales before and after hyperalignment. This approach is a variation of the "fingerprinting"[10,45] approach, whereby measured individual differences are more reliable if a subject is more similar to themselves across split-halves than to other subjects**. A.** Spatial distribution of reliability scores before and after hyperalignment at the fine and coarse scales, as visualized on the cortical surface for each parcel. **B.** The reliability of individual differences increases after hyperalignment for all parcels. 99% of fine connectivity profiles (darker) are more reliable than coarse ones (lighter) regardless of alignment type. **C.** Box-and-whisker plots showing the distribution of IDM reliability scores across parcels within connectome type. Box shows first quartile, median, and third quartile of distribution. Whiskers represent 1.5 times the interquartile range, and points represent outlier values.

Genetics contribute most strongly to the coarse-scale connectome

We asked whether the more reliable fine-scale connectome simply reflected the same information about cortical functional architecture at higher magnification or a different class of information that may be more or less heritable or more or less reflective of experience. We investigated this question by calculating the heritability of the two coarse-grained and the two

fine-grained connectomes. We hypothesized that heritable factors determine the skeletal attributes of the connectome and are more evident at the coarse spatial scale[4,27,28], whereas the detailed configurations of connectomes may develop under the influence of less heritable factors, such as experience, and are reflected at a finer spatial scale.

The heritability analysis used RSFC data from 778 subjects comprising 219 dizygotic twin pairs and 170 monozygotic twin pairs (see breakdown in Table S1). As in prior analyses, the connectivity hyperalignment model was trained on 200 unrelated subjects, then the connectomes of the 778 twin subjects were hyperaligned to this model. Functional connectomes of vertex-granularity are an inherently high-dimensional phenotype. To explicitly model the heritability of this phenotype, we used a multidimensional estimate of heritability[24] to model both the phenotypic similarity matrix between participants as well as the genetic kinship matrix (see Multidimensional heritability estimation for more details).

We find that both the anatomically-aligned and CHA-aligned coarse-grained connectomes were more heritable than the more reliable fine-grained connectomes ($p < 0.0001$) (Figure 3). At the coarse scale, anatomically-aligned functional connectomes are significantly more heritable than hyperaligned connectomes (AA $h^2 = 0.198 \pm 0.05$; CHA $h^2 = 0.161 \pm 0.04$; $p < 0.0001$), with 96% of parcels showing greater heritability. These results indicate that connectivity information aligned coarsely based on anatomical features are under strong genetic control, consistent with previous studies showing genetic control over cortical anatomy in children[20] and network-level RSFC[2].

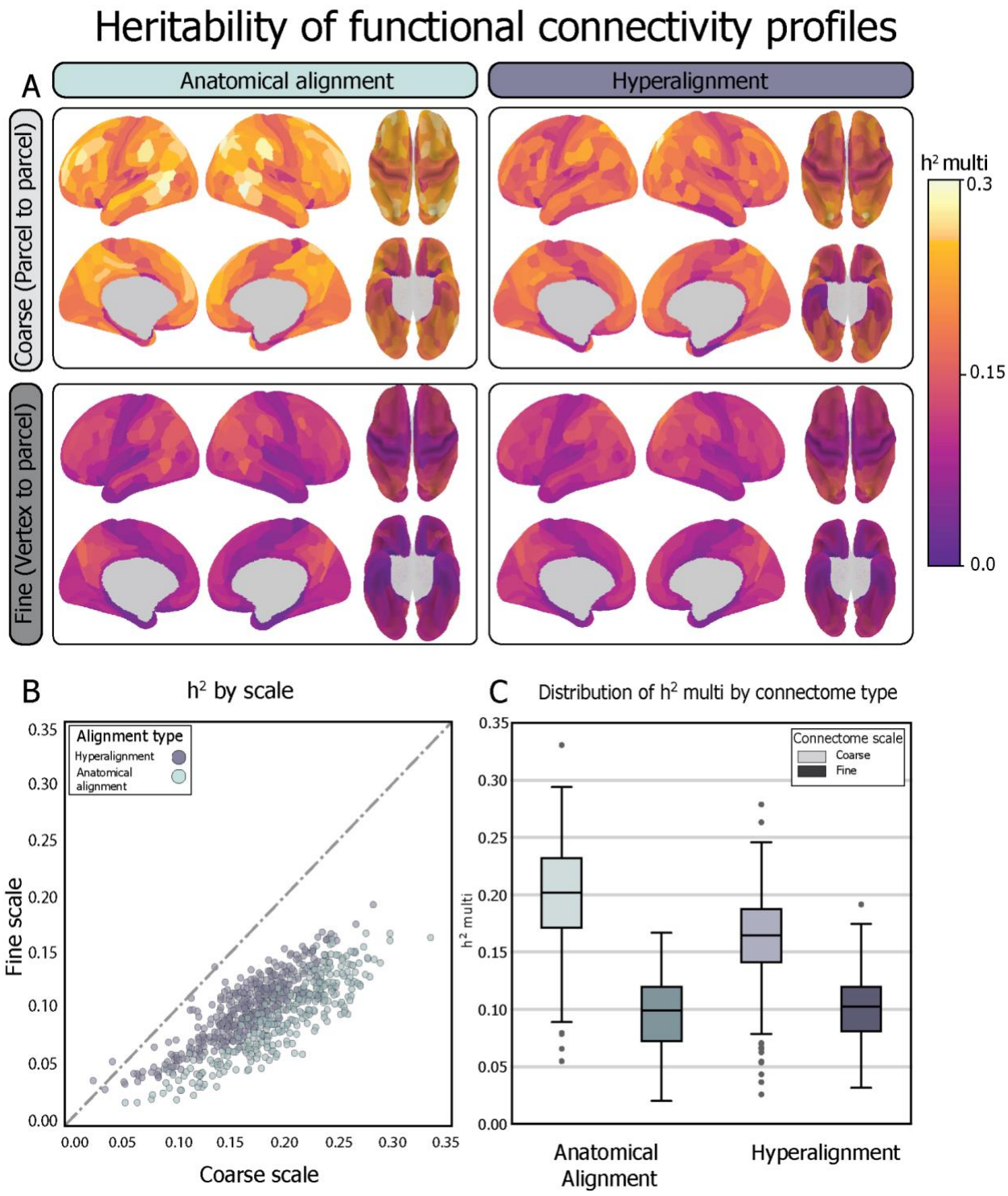

Figure 3. Heritability of functional connectivity profiles

Procedure: Heritability of functional connectivity profiles between regions (defined with the Glasser parcellation[33]) was estimated using a multidimensional heritability model[24] using resting-

state fMRI data from 778 9–10-year-olds (170 MZ pairs and 219 DZ pairs). Functional connectivity between a given parcel and all other parcels in the brain was calculated at fine and coarse granularities, before and after connectivity hyperalignment. The coarse-grained connectivity profiles aligned based on cortical anatomy are the most heritable. **A.** Spatial distribution of h^2-multi scores before and after hyperalignment at the fine and coarse scales, as visualized on the cortical surface for each parcel. **B.** For both anatomically-aligned and hyperaligned data, connectivity profiles are more heritable when calculated at the coarse scale than the fine scale (99.6 percent of the time). **C.** At the coarse scale, the anatomically aligned connectivity profiles are more heritable than the hyperaligned ones, but not at the fine scale, which is under comparatively minuscule genetic control. Box-and-whisker plots showing the distribution of h^2-multi across parcels within connectome type. Box shows first quartile, median, and third quartile of distribution. Whiskers represent 1.5 times the interquartile range, and points represent outlier values.

Prediction of neurocognitive abilities

We next asked whether the reliable individual differences in the fine-scale connectomes that have low heritability reflect differences in cognitive abilities that are fostered by experience. Compared with brain structure, complex psychological traits are less heritable, but cognitive abilities are among the most heritable dimensions of human behavior[46]. Heritability (h^2) of cognitive abilities varies by domain and increase with age, with higher estimates for general cognitive ability (h^2 =0.54–0.85 at 10–12 years[47] and h^2 = 0.60–0.73 at 8–21 years[48]) than for specific cognitive abilities like learning/memory[49] (h^2 = 0.18–0.55 at 8–21 years[48] and h^2 = 0.39 at 18–67 years[50]), which tend to be more sensitive to experiential factors. In this proof-of-

principle analysis, we leveraged the variation in heritability between learning/memory and general cognitive ability to examine the functional significance of our heritability and reliability findings. Previous work[51] using data from the first release of baseline ABCD data to determine components of higher-cognitive abilities during development calculated composite neurocognition component scores using a Bayesian Probabilistic Principal Components Analysis (BPPCA) model over the NIH Cognitive Toolbox tasks administered in the ABCD study and released as a single score for each component per participant in the data repository. Here, we focused on the composite scores for general cognitive ability and learning/memory. Since learning/memory is regarded as less heritable than general cognitive ability, we leveraged the variability of heritability in connectivity to predict variably-heritable cognitive phenotypes[48,49]. Given that CHA improves reliability of individual differences in the fine-scale connectome, we predicted that CHA fine connectomes would capture more variance in both cognitive traits than the CHA coarse, AA coarse, or AA fine connectomes. Moreover, we predicted that the most heritable connectome (AA coarse) would reflect more variance in a more heritable cognitive trait (general cognitive ability) relative to a less heritable one (learning/memory).

We used a principal components analysis ridge regression to predict scores on these two cognitive domains from connectivity profiles at each scale. Models were trained using the individual differences matrices (IDMs) across 526 unrelated subjects, computed for each scale, alignment, and parcel. Crucially, predictions based on IDMs ensure that all models are receiving data with the same number of features, regardless of connectome type, since IDMs are 526 subjects by 526 subjects where each cell is a pairwise correlation distance between the connectomes of two subjects. We used a nested cross-validation procedure to tune

hyperparameters (number of PCs and α) then apply the model to predict loadings from unseen subjects (see Neurocognition PC prediction analysis for more details). Model scores are presented as R2 between predicted scores and true values, and score significance was assessed by repeating this analysis with permuting behavioral scores (1,000 iterations per model) to create a null distribution. Model scores were compared across connectome types using 10,000 bootstrap iterations with resampling.

Overall, hyperaligned fine-scale connectomes best predicted individual differences in cognitive performance (i.e., both general cognitive ability and learning and memory), and the degree to which the coarse connectome also contributed to prediction was associated with the heritability of the trait. The more heritable psychological trait of general cognitive ability was similarly predicted by CHA fine, AA coarse, and AA fine connectomes (average $R^2 \pm$ s.d. across parcels: CHA fine = 0.0133 ± 0.021; AA fine = 0.0134 ± 0.020; AA coarse = 0.0124 ± 0.018; Bonferroni-corrected p-values reported from permutation test with 10,000 iterations: CHA fine vs. AA fine p= 1.0; CHA fine vs. AA coarse p = 1.0; AA fine vs. AA coarse p = 0.39) (Figure 4), indicating that the information content carried in each of these connectomes predicts general cognitive ability. Compared with the other three connectomes, CHA coarse connectomes predicted significantly less variance in general cognitive ability ($R^2 = 0.006 \pm 0.02$; CHA coarse vs. CHA fine $p < 0.0001$; CHA coarse vs. AA fine $p < 0.0001$; CHA coarse vs. AA coarse $p < 0.0001$), suggesting that functionally aligning fine-scale information then smoothing over the functional information space actually diminishes the specificity of the information. After performing permutation tests at each parcel and thresholding at $p < 0.01$, 42%, 42.5%, 30.5%,

and 43% of parcels predicted general cognitive ability significantly greater than chance at the AA coarse, AA fine, CHA coarse, and CHA fine scales, respectively (Figure S6).

Learning/memory is regarded as a less heritable psychological trait ($h^2 = 0.36–0.56$)[48], so we hypothesized that the information content of the coarse connectomes (the more heritable information) would contribute less to the prediction of this trait relative to the fine connectomes (the more reliably idiosyncratic information). Indeed, prediction of learning/memory scores were significantly higher for the CHA fine connectome than the other connectome types (average R^2 ± s.d. across parcels: CHA fine = 0.018 ± 0.012; CHA coarse = 0.011 ± 0.014; AA fine 0.008 ± 0.014; AA coarse 0.007 ± 0.014; Bonferroni-corrected p-values: CHA fine vs. CHA coarse $p < 0.0001$; CHA fine vs. AA fine $p < 0.0001$; CHA fine vs. AA coarse $p < 0.0001$; CHA coarse vs. AA fine $p = 0.007$; CHA coarse vs. AA coarse $p < 0.0001$; AA fine vs. AA coarse $p = 0.529$) (Figure 4). The gap in the percentage of parcels capturing a significant amount of variance was also more pronounced for this trait; 30%, 33%, 39%, and 61% for AA coarse, AA fine, CHA coarse, and CHA fine.

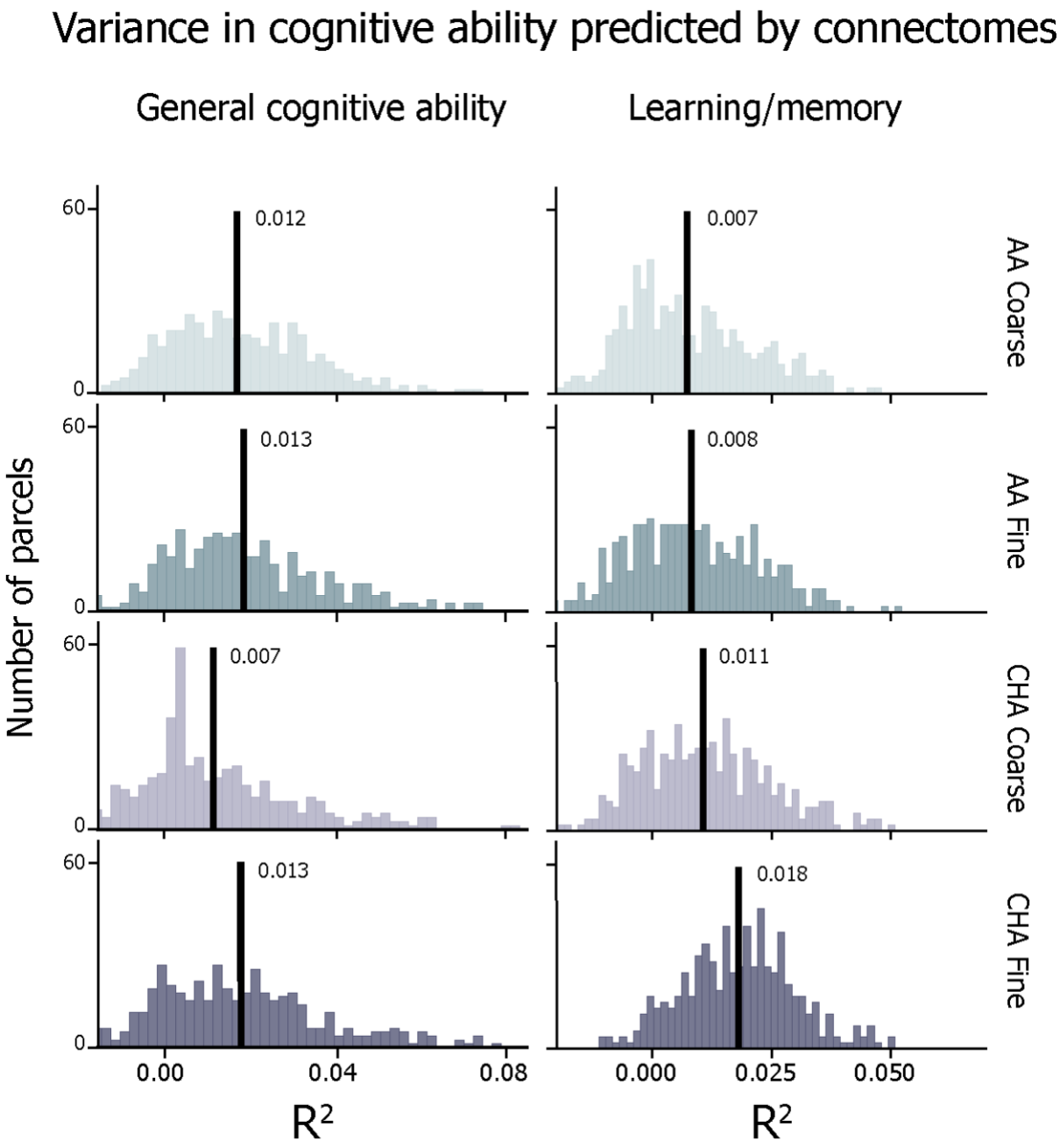

Figure 4: Prediction of neurocognitive PC loadings.

Distribution of R^2 values across all parcels for prediction of general cognitive ability (left) and learning/memory (right). Histogram heights correspond to density of scores and lines represent the mean of the score distribution. For the purpose of distribution matching, R^2 values are not

thresholded here; thresholded R^2 values mapped to the cortical surface are displayed in Figure S6.

Discussion

In this study, we investigated whether heritable and experiential factors have dissociable effects on the development of coarse- and fine-grained levels of functional organization in the developing connectome. We hypothesized that the coarse-grained structure of connectivity between cortical regions — the scaffolding of the connectome — would be under stronger genetic control, whereas the fine-grained structure of local variations in connectivity would be shaped more by individual-specific learning and experience. We improved access to individual differences in fine-grained connectivity by applying connectivity hyperalignment (CHA) to resting-state fMRI data in a large sample of children from the ABCD® dataset. Our study presents the first example of defining and applying a functional common space to a developmental cohort. This represents an important advancement in developmental neuroimaging as it disentangles meaningful individual differences from misaligned cortical anatomy or measurement noise.

Using a normative set of 200 children's brains, we built a fine-grained model connectome and hyperaligned a separate set of 915 children to that template. Before hyperalignment, the connectivity profiles of anatomically-aligned vertices exist in distinct, individual representational spaces and are, therefore, both less reliable and less predictive of behavioral traits. Hyperalignment resamples an individual's vertex-wise connectivity profiles into the model connectivity profiles, which affords meaningful comparisons of fine-grained profiles across individuals. Prior literature has relied upon anatomical alignment, or matching children's data to

a common anatomical template brain, then applying a parcellation (commonly defined on adult brains) to extract an average (coarse) timeseries for each predefined region[11,15,31,52]. By averaging connectivity profiles across neighboring vertices in a region, one can factor out misaligned fine-grained variation to reveal the scaffolding of the coarse-grained connectome, but this obscures the information contained in fine-grained variations. We considered multiple connectome types — coarse- and fine-grained, pre- and post-CHA — to understand the effects of genetics and experience at different scales of connectivity.

Using CHA, we revealed reliably idiosyncratic patterns of fine-scale functional connectivity. The coarse scale connectome (AA coarse) shows only moderately reliable idiosyncrasies (mean Pearson's $r = 0.34$), versus the CHA fine connectome's mean reliability of $r = 0.86$ (Figure 2). Across the cortex, individual differences in fine-scale functional connectivity were more reliable than in coarse-scale, suggesting that traditional, coarse alignment diminishes spatially-resolved topographies of information transfer. By estimating the heritability of functional connectivity at each scale and alignment in monozygotic and dizygotic twins, we showed that idiosyncrasies in the fine-scale connectomes were dissociable from idiosyncrasies in the coarse scale connectome. Multiscale heritability analysis of coarse scale, anatomically aligned connectomes attributed about 20% (5.47–33.06%) of variance to genetic relatedness, which converged with our expectations based on adult coarse RSFC estimates[2,3,24] and how neuroimaging phenotypes increase in heritability with age[4,19]. At the fine scale, h^2 estimated dropped to around 10% regardless of alignment technique (CHA: 3.1–19.2%, AA: 2.0–16.67%), suggesting that at the fine scale, idiosyncrasies in RSFC were likely more associated with unique experience than genetics (Figure 3). These results supported our hypothesis: whereas individual differences in

fine-grained connectivity after hyperalignment were dramatically *more* reliable than differences in coarse-grained connectivity, they were dramatically *less* heritable, indicating a dissociation between the spatial scales of heritable and reliable patterns of functional connectivity.

Our final analysis examined the behavioral relevance of this dissociation. The most reliably idiosyncratic (CHA fine) and most heritable (AA coarse) connectomes were similarly predictive of general cognitive ability, a canonically heritable cognitive trait. In contrast, the most reliably idiosyncratic connectome (CHA fine) was most predictive of a less heritable cognitive trait (learning/memory) (Figure 4). Past studies using coarse RSFC from the ABCD dataset were limited in their ability to predict general cognitive ability and not learning/memory scores[11]. By applying CHA, we uncovered individual-specific patterns of functional connectivity that better predict a presumably less heritable, more experience-related cognitive trait (learning/memory).

Taken together, we demonstrate a link between reliable, heritable, and predictive scales of functional connectivity and highlight the importance of nuanced, multi-scale connectivity analyses for holistically understanding individual differences during development. Our findings dovetail with the interactive specialization framework of functional brain development, which states that the development of the functional connectome is not solely determined by a blueprint, but the interaction of a heritable template of connections and individualized experience[53]. We provide neural evidence in support of this framework: the coarse connectome serves as a heritable blueprint which represents more heritable cognitive phenotypes. Fine-scale connectomes capture *similar* information as the coarse (as AA coarse never out-predicts CHA

fine), but the organization of fine-scale information is remixed in a way that diverges from the heritable blueprint and individualized, experience-driven phenotypes.

Recent work has recognized the need for massive numbers of subjects and samples to reliably associate brain phenotypes with behavior, specifically in RSFC of developmental cohorts[31]. The need for massive cohorts could be attributed to the specifics of neuroimaging phenotypes. However, leveraging machine learning advances including multivariate models, functional alignment, or individual-specific functional atlases as opposed to group-average atlases is one approach to improving prediction[12,15,54,55,34,35,56]. Our study demonstrates the power of hyperalignment as a tool for understanding developing individual differences in brain and behavior. The hyperalignment model was trained on RSFC from 200 children and tested on a separate cohort, using under 20 minutes of resting-state data per subject. The prediction results assure that the increased reliability of individual differences was driven by generalizable, shared signals in the hyperalignment model rather than overfitting to subject-specific signals or simply higher-dimensional data, since CHA improved reliability over AA at the fine-scale as well. By performing all subsequent analyses on pairwise (dis)similarity matrices, we further ascertain that our results are driven by the information content represented in different connectomes, rather than the dimensionality difference between coarse- and fine-grained connectomes.

This study should be interpreted in light of potential limitations. Though statistically significant, our predictions accounted for relatively low variance in behavioral measures relative to similar studies in adults[10,12,57]. While task-based FC is more stable and predictive of behavior than RSFC among adults[9,12,38,58], this requires sufficient amounts of high-quality data, notably difficult to

collect in children[29,59]. RSFC measures appear to be reliable in the ABCD dataset[52], whereas the task fMRI has known reliability limitations[29]. Furthermore, RSFC has been shown to be more heritable than task-based FC[19], suggesting that the added cognitive load of a task introduces idiosyncrasies in information processing less attributable to genetics similarity.

Our choice to focus on two composite scores of neurocognition (general cognitive ability and learning/memory), previously identified in Thompson et al. (2019)[51], should be viewed as a proof-of-principle analysis relating the heritability and reliability of individual differences in neuroimaging phenotypes to differentially heritable behavioral phenotypes. H^2 of general cognitive ability and learning/memory in the present cohort (Figure S4) were both higher and more similar to one another than the values reported in the literature[48–50,60]. This could be because our sample has a diverse racial background and restricted age range, in contrast to previous research based on predominantly European descent[60–63] with a larger age range[47–50]. Our predictions align most closely with Mollon et al. (2021)[48], which considered a more racially-diverse cohort, potentially enhancing generalizability beyond Caucasians, and an overall younger sample than prior studies, overlapping with our sample demographics. We also replicated our heritability results using data from the entire cohort (n = 9,519) to rule out potential concerns on sampling bias (Figure S4). Across the tasks, those loading more strongly onto the general cognitive ability component (*pic vocab, reading*) showed stronger heritability compared to tasks loading more strongly onto the learning/memory component (*card sort, picture*) (Figure S5). Notably, even with overlap in the two components (i.e., *list sorting* task loading on both), we still see distinct brain-based predictions associated with heritability.

This paper presents several novel findings. First, hyperalignment can be used as a tool to improve the reliability and behavioral relevance of functional connectivity in children. After hyperalignment, reliability of individual differences in RSFC is improved at the fine-scale relative to the coarse scale, but the heritability of these signals is weakened. Finally, we present a potential application of this dissociation in the fine and coarse scale connectomes to show how the heritability of RSFC relates to ability to predict behavior based on the heritability of behavioral traits. With the substantial twin cohort, behavioral testing, and longitudinal neuroimaging data included in the ABCD study, future work could investigate the connection between heritability and predictivity of functional connectivity over time, as the heritability of both neurocognitive measures and neuroimaging-based phenotypes increase with age[1,4,21,64]. Moreover, this approach could be used to investigate how functional topographies reflect cognitive development over time, by hyperaligning a subject to themselves at multiple timepoints. In conclusion, the current study shows that by breaking apart the pieces of the functional connectome into their coarse and fine structures, we can better understand how these scales interact to scaffold and instantiate reliable idiosyncrasies in brain and behavior during development.

Materials and methods

Participants

We considered data from the 11,875 children included in the Adolescent Brain Cognitive Development (ABCD) Study®[16] , data release 2.0.1. The ABCD Study is a longitudinal study with 21 sites around the United States and aims to characterize cognitive and neural development with measures of neurocognition, physical and mental health, social and emotional function, and

culture and environment. The ABCD Study obtained centralized institutional review board (IRB) approval from the University of California, San Diego, and each site obtained local IRB approval. Ethical regulations were followed during data collection and analysis. Parents or caregivers provided written informed consent, and children gave written assent. Four leading twin research centers at the University of Minnesota, Virginia Commonwealth University, University of Colorado-Boulder, and Washington University in St. Louis comprise the ABCD Twin Hub. Each site enrolled approximately 200 same-sex monozygotic or dizygotic twin pairs as well as singletons[17]. Their inclusion in the ABCD study affords unique access to the causal interrelation between genetics, environment, brain function, and cognition during development[1,4,17].

The present study used imaging and behavioral data from a subset of n=1,115 subjects from the original 11,875 subjects. Included subjects were enrolled in the University of Minnesota, Washington University in St. Louis, and University of Colorado-Boulder sites, which all use 3T Siemens MRI scanners. We excluded Virginia Commonwealth University, the fourth Twin Site, as it uses a GE scanner, a potential confound in the current study[16]. ABCD study-wide exclusion criteria include a diagnosis of schizophrenia, moderate to severe autism spectrum disorder, intellectual disabilities, major and persistent neurological disorders, multiple sclerosis, sickle cell disease, seizure disorders like Lennox-Gastaut Syndrome, Dravet Syndrome, and Landau Kleffner Syndrome, or substance abuse disorders at time of recruitment. Subjects with mild autism spectrum diagnosis, history of epilepsy, traumatic brain injury, and MR incidental findings were excluded from the present analysis.

Resting state fMRI data collection

Structural and functional data from the three included sites were acquired using Siemens Prisma 3T scanners with a 32-channel head coil. Detailed acquisition parameters are previously described in the literature[16,65]. Scan sessions consisted of a high-resolution (1 mm^3) T1-weighted image, diffusion weighted images, T2-weighted spin echo images (1 mm^3), resting-state fMRI (rs-fMRI), and task-based fMRI. We utilized rs-fMRI solely in this study. rs-fMRI data were collected with an echo-planar imaging sequence with 2.4 mm voxels, TR = 800 ms, TE = 30 ms, and multiband slice acceleration factor = 6. Participants completed up to four runs of 5-minute resting state scans. Framewise integrated real-time MRI monitoring (FIRMM[66]) was used to monitor subject head motion during data collection, and scan operators may have stopped resting-state data collection after three runs if 12.5 min of low-motion resting-state data had been collected.

Additional exclusions were made based on poor structural scan quality (determined with curated data release 2.0.1 sheet *freesqc01.txt*) or low quality/high motion resting state fMRI (determined as a score of zero for *fsqc_qc* or greater than one for *fsqc_qu_motion*, *fsqc_qu_pialover*, *fsqc_qu_wmunder*, or *fsqc_qu_inhomohgeneity*), as reported in prior studies[54]. Participants with fewer than 900 TRs of rs-fMRI data passing these measures for FreeSurfer reconstruction were also excluded. ABCD Data Release 2.0.1 used FreeSurfer version 5.3 for quality control checks[65]. After filtering, we used resting state fMRI and behavioral data from 1,115 unique subjects (552 male), including 170 pairs of monozygotic (MZ) twins, 219 pairs of dizygotic (DZ) twins, and 337 singletons. All twin pairs were same-sex, and all subjects were between 9 and 10

years old. Included singletons were also balanced for ancestry, ethnicity, sex, and pubertal development with twins (Table S1).

Preprocessing

rs-fMRI data were downloaded via the DCAN Labs ABCD-BIDS Community Collection[67] (NDA Collection 3165). This is a regularly updated dataset of ABCD Brain Imaging Data Structure (BIDS)[68] version 1.2.0 pipeline inputs and derivatives, using source data from the ABCD Study participants baseline year 1 arm 1 DICOM imaging data that passed initial acquisition quality control from the ABCD Data Analysis and Informatics Center (DAIC)[65] and retrieved from the NIMH Data Archive (NDA) share of ABCD fast-track data (NDA Collection 2573). DICOMs were converted to BIDS input data using Dcm2Bids[69], which reorganizes NiftiImages produced with dcm2niix[70]. Raw images were preprocessed using the DCAN Labs ABCD-BIDS MRI processing pipeline[71] (for details, see github.com/DCAN-Labs/abcd-hcp-pipeline; osf.io/89pyd), which is based on the Human Connectome Project (HCP) Minimal Preprocessing Pipeline[72] with additional modifications specifically for the ABCD dataset and summarized below.

The first stage of the pipeline, PreFreeSurfer, performed brain extraction, alignment, and N4 bias field correction on the T1w and T2w images. The second stage, FreeSurfer[73,74], segmented the resulting T1w images and identified tissue boundaries to register to a FreeSurfer template and produce brain masks. The third stage, PostFreeSurfer, used the brain masks to register T1w images to MNI space using ANTs symmetric image normalization method[75]. Surfaces were then transformed to standard space using spherical registration and converted to CIFTI format along

with the standardized brain volumes. Multimodal surface registration was performed with MSM-sulc. The fMRIVolume stage performed functional image distortion correction using reverse phase-encoded spin echo images to correct for local field inhomogeneities. Eta squared values were computed for each image to a participant-level average of all field maps, and the pair with the highest value (i.e., most representative of the average) was selected to avoid potential motion confounds. Finally, the fMRISurface stage performed 2-mm full-width half-max spatial smoothing.

DCAN BOLD Processing[76] was used to perform standard data processing. First, fMRI data were demeaned and detrended with respect to time. Covariates of no interest were regressed from the data, including mean white matter, cerebrospinal fluid, overall global signal, mean grayordinate timeseries, and 6-movement variables (X,Y,Z translation and roll, pitch, yaw rotation). Timeseries data were then band-pass filtered between 0.008 and 0.09 Hz using a 2nd order Butterworth filter. Data were then filtered for respiratory motion for the frequencies (18,582 to 25.726 breaths per minute) of the respiratory signal, which has been shown to improve the stability of framewise displacement (FD) estimates[77]. “Bad” frames, where motion exceeds FD of 0.3 mm, were removed when demeaning and detrending such that denoising betas were only calculated for “good” frames. For the band-pass filtering, interpolation was used to replace those frames, so that pre-processing of the timeseries only includes “good” data but avoids aliasing due to missing timepoints. Finally, the filtered timeseries were normalized and concatenated across runs. The derivatives used in this analysis are *ses-baselineYear1Arm1_task-rest_bold_desc-filtered_timeseries.dtseries.nii.

Connectivity hyperalignment

We used connectivity hyperalignment[38] to functionally-align fine-scale connectivity information across subjects. Given the small quantity (1480 ± 142 TRs; mean ± std) of resting state fMRI data available per subject, we chose to train the hyperalignment model common space using a cohort of 200 subjects who were then excluded from further analysis. These 200 training subjects were singletons enrolled at one of the three included sites and were matched with twin subjects on gender, pubertal development, age, and race/ethnicity (Table S1). The remaining 915 subjects (including the 389 twin pairs and 137 singletons) were used for subsequent analyses. Crucially, the hyperalignment model space never saw data from any subjects included in analyses during training.

We followed the same connectivity hyperalignment procedure for whole-cortex parcellation data as in our previous study[12]. We used the average timeseries for each of the 360 regions in the Glasser cortical parcellation[33] as connectivity targets and the vertices in each parcel as connectivity seeds. For each parcel we computed a fine-scale connectivity matrix as the correlation between each of the vertices within the parcel and the average regional timeseries of the other 359 regions in the parcellation. For example, for a parcel with 430 vertices, its fine-scale connectivity matrix would be a matrix of dimensions 430 by 359 correlation coefficients, whereas its coarse-scale connectivity profile would be a vector of 359 correlation coefficients (Figure 1B).

For each region[36], we trained a separate high-dimensional common model space based on the fine-scale functional connectomes of the 200 training subjects. The dimensionality of the model

space is equal to the number of vertices, but the model dimensions correspond to shared functional connectivity properties across individuals instead of anatomical locations[6]. After the model dimensions were learned, we discarded training subjects' data from downstream analyses. We derived invertible transformation matrices for the remaining subjects' connectomes into the model space to map vertex timeseries from the anatomically-defined dimensions into the functionally-defined dimensions.

Functional connectivity profiles

After aligning the test data into a common functional space, we used functional connectivity profiles to summarize a brain region's correlation with the rest of the cortex. We defined fine-scale functional connectivity profiles as above, as the correlation between the timeseries of all 59,412 vertices in the cortex with the average timeseries of each parcel, resulting in a matrix of 59,412 by 360 correlation coefficients per subject. We also defined coarse-scale functional connectivity profiles as the correlation between the average timeseries for all pairs of parcels, resulting in a matrix of 360 by 360 correlation coefficients per subject (Figure 1B). The fine-scale and coarse-scale connectomes were computed on data pre- and post-hyperalignment for each subject to evaluate the effect of functional alignment and connectome granularity on heritability, reliability, and predictivity.

Individual differences matrix (IDM) reliability

Given the high levels of noise and low reliability associated with developmental neuroimaging data[29,43,59,78,79] as well as smaller (vertex-resolution) connectivity seeds[7], we used hyperalignment to improve the reliability of individual differences in our data. That is, by finding a space that

aligns patterns of functional connectivity across subjects (within anatomically constrained parcels), we correct more thoroughly for anatomical variability and improve access to reliable individual differences[6,56]. We calculated the reliability of functional connectomes before and after hyperalignment as follows. For 526 unrelated subjects, we computed fine-scale functional connectomes from split-half timeseries (742 ± 71 TRs). We derived transformation matrices to rotate these connectomes into the common space separately, then aligned the split timeseries data using those transformations. We then computed functional connectivity profiles, as explained above, for each half separately. For each parcel at the fine and coarse scale separately, we used the vectorized functional connectivity profiles before and after hyperalignment and computed individual differences matrices (IDM) for each data split. These are subject-by-subject pairwise dissimilarity matrices, where each value in the matrix is the correlation distance (1 - Pearson's r) between two subjects' regional connectivity profiles. After computing IDMs, we took the upper triangle of the IDM and correlated them (Pearson's r) to measure the reliability of the individual differences in the functional connectomes across the split halves[41]. This metric reflects the reliability of the idiosyncrasies in a subject's functional connectomes, where subjects are more similar to themselves across split halves than they are to any other subject. We used a Mantel test[80,81] to perform statistical tests on IDMs with 10,000 permutations.

Multidimensional heritability estimation

Functional connectomes at vertex-granularity are an inherently high-dimensional phenotype; when dimensionality of the phenotype is collapsed, the reliability of individual differences decreases[41]. To offer greater statistical power in analyzing the heritability of this high-dimensional phenotype, we used a multidimensional estimate of heritability[24,25] to summarize the

degree to which functional connectivity profiles for each parcel are under genetic control. We also investigated whether the alignment and granularity of the connectomes impact their heritability, which would indicate that the information highlighted by that type of connectome calculation is differentially impacted by genetics. Genetic kinship was estimated with SOLAR Kinship2[82].

Neurocognition PC prediction analysis

Neurocognition principal components (neurocog PCs)[51] were derived from the neurocognitive battery included in the ABCD study. The neurocognitive battery includes the NIH Toolbox cognition measures covering episodic memory, executive function, attention, working memory, processing speed, and language abilities. The neurocog PCs were derived with a Bayesian Probabilistic Principal Components Analysis, which revealed a three-component solution. The three components roughly corresponded to general cognitive ability, executive function, and learning/memory. Since the NIH Toolbox tasks that canonically measure executive function did not load onto the executive function component in this solution, we excluded this component from our analyses, instead focusing on general cognitive ability and learning/memory. Tasks loading onto the general cognitive ability component include Toolbox Picture Vocabulary, Toolbox Oral Reading test, List Sort Working Memory task, and Little Man task. Tasks loading onto the learning/memory component include the Toolbox Picture Sequence Memory task, the RAVLT total number correct, and the List Sort Working Memory task. Heritability of composite scores were estimated with SOLAR Polygenic[82] including sex, age, ethnicity, and site as covariates.

We predicted individual subjects' scores onto the neurocognition principal components based on individual differences in RSFC from our cohort of 526 unrelated subjects using a principal component ridge regression adapted from our previous study[12]. For each parcel, scale, and alignment, we computed subject-wise individual differences matrices (IDMs) of functional connectivity over the entire resting-state timeseries. Next, we ran a principal components analysis (PCA) over the IDM to decompose the IDM into main orthogonal dimensions along which individuals' connectivity profiles differ from one another. We then trained a ridge regression model to predict neurocog scores from the decomposed IDM. Models were trained and tested using nested cross-validation, where the inner fold optimized regression model parameters (including the number of IDM PCs retained and α) across three sub-folds and the outer fold scored the selected model on a held-out subject. Candidate regression model parameters were distributed evenly on a logarithmic scale, from 10 to 320 PCs and no PCs (no dimensionality reduction), and α chosen from 121 values between 10^{-20} to 10^{40}. Models were evaluated using the cross-validated coefficient of determination R^2, which shows the variance in neurocog scores accounted for by the prediction models. To assess statistical significance of model performance against chance, we used permutation testing with 1000 iterations of shuffling the behavioral scores.

Data availability

The ABCD study is longitudinal, so the data repository changes over time and can be found here: https://nda.nih.gov/abcd. In the current study, we used the ABCD data release 2.0.1, downloaded via ABCD-BIDS Community Collection[67] NDA Collection 3165.

Code availability

ABCD data preprocessing code can be found here: https://github.com/DCAN-Labs/abcd-hcp-pipeline. ABCD data processing code can be found here: https://github.com/DCAN-Labs/dcan_bold_processing. Code for running the multiscale heritability analysis can be found here: https://github.com/kevmanderson/h2_multi. Code for running the nested PCA ridge regression was based off: https://github.com/feilong/IDM_pred. All analysis code specific to this study will be released upon publication.

Acknowledgements

This project was supported by the National Science Foundation Graduate Research Fellowship Award # 2139841 to Erica L. Busch.

Data used in the preparation of this article were obtained from the Adolescent Brain Cognitive Development (ABCD) Study (https://abcdstudy.org), held in the NIMH Data Archive (NDA). This is a multisite, longitudinal study designed to recruit more than 10,000 children age 9-10 and follow them over 10 years into early adulthood. The ABCD Study is supported by the National Institutes of Health and additional federal partners under award numbers U01DA041048, U01DA050989, U01DA051016, U01DA041022, U01DA051018, U01DA051037, U01DA050987, U01DA041174, U01DA041106, U01DA041117, U01DA041028, U01DA041134, U01DA050988, U01DA051039, U01DA041156, U01DA041025, U01DA041120, U01DA051038, U01DA041148, U01DA041093, U01DA041089, U24DA041123, U24DA041147. A full list of supporters is available at https://abcdstudy.org/federal-partners.html. A listing of participating sites and a complete listing of the study investigators can be found at https://abcdstudy.org/consortium_members/. ABCD

consortium investigators designed and implemented the study and/or provided data but did not necessarily participate in analysis or writing of this report. This manuscript reflects the views of the authors and may not reflect the opinions or views of the NIH or ABCD consortium investigators.

This research also benefited from the ABCD Workshop on Brain Development and Mental Health, supported by the National Institute of Mental Health of the National Institutes of Health under Award Number R25MH120869 and by UG3-DA045251 from the National Institute of Drug Abuse.

Author Contributions

Conceptualization, ELB, KMR, MDR, MF, JH, RW, and BJC; Methodology, ELB, MF, JH, and KMA; Software, ELB, KMA, and MF; Validation, ELB, KMA, MF, and JH; Investigation, ELB; Writing - Original Draft, ELB, MF, and BJC; Writing - Review & Editing, ELB, KMR, MDR, RW, KMA, MF, JH, and BJC; Visualization, ELB and KMR; Supervision, MF, JH, and BJC; Funding acquisition, BJC.

Declaration of interests

KMA is an employee of Neumora Therapeutics.

Supplemental tables and figures

Table S1: Cohort Breakdown

	Total Included	Monozygotic Pairs	Dizygotic Pairs	Unrelated Test	Unrelated Train
Total	1,115	170	219	526	200
Site 20	387	75	86	184	60
Site 21	371	34	81	166	90
Site 22	357	75	68	176	50
Age (mo) (*interview_age*)	121.6	122.5	122.0	121.6	120.7
% Female (*gender*)	50%	52%	50%	50%	50%
Ancestry: African (*AFR*)	0.127	0.092	0.118	0.113	0.204
Ancestry: European (*EUR*)	0.805	0.825	0.826	0.814	0.733
Ancestry: East Asian (*EAS*)	0.020	0.016	0.016	0.021	0.025
Ancestry: (*AMR*)	0.049	0.067	0.040	0.052	0.038
Ethnicity (*race_ethnicity*)	1.667	1.659	1.63	1.73	1.58

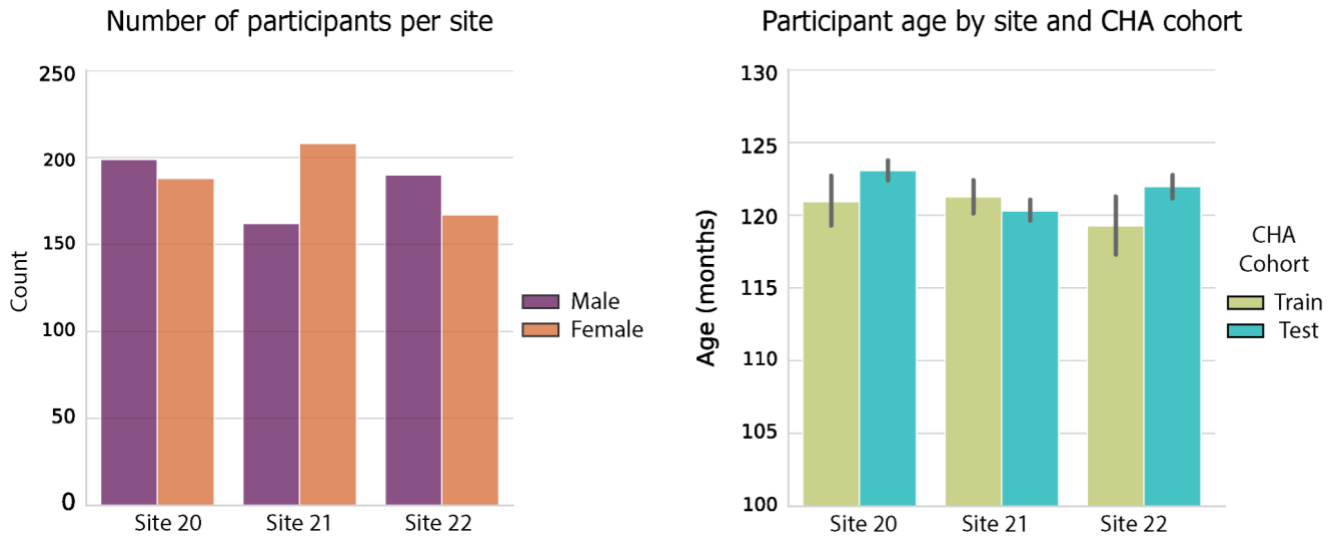

Figure S1: Participant information.

Left: Number of participants included from each of the three selected sites, separated by gender. **Right**: Participants were broken into two cohorts for training/testing the CHA model. 200 total unrelated participants reflective of within-site age, demographics, and ancestry (see below figures; 60, 90, and 50 from each respective site) were selected to train the CHA model. The remaining participants were used in subsequent tests.

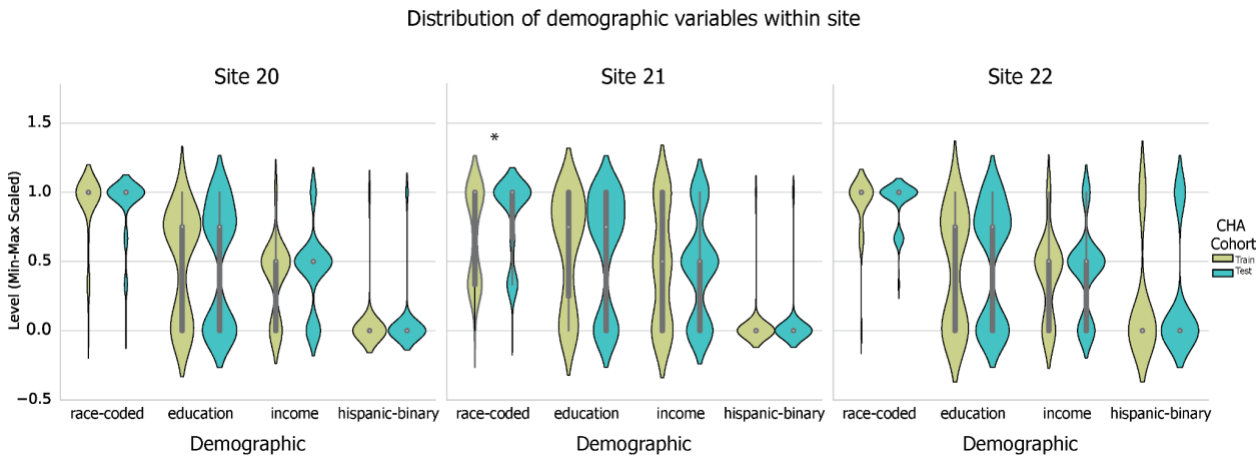

Figure S2: Participant demographics.

The three sites significantly differed in mean demographic attributes, including a four-level race model, parental education level, parental income, and Hispanic identity. To respect this diversity and sample a wide range of demographics, we selected CHA training subjects to reflect sample demographics along these four dimensions. Shown here are the distributions of participants' scores, scaled to a 0–1 range for visualization, for the participants allocated for CHA train or test cohorts. Significance of differences along each dimension between CHA cohorts were tested with a two-tailed independent samples t-test and * denotes $p < 0.05$ after Bonferroni correction.

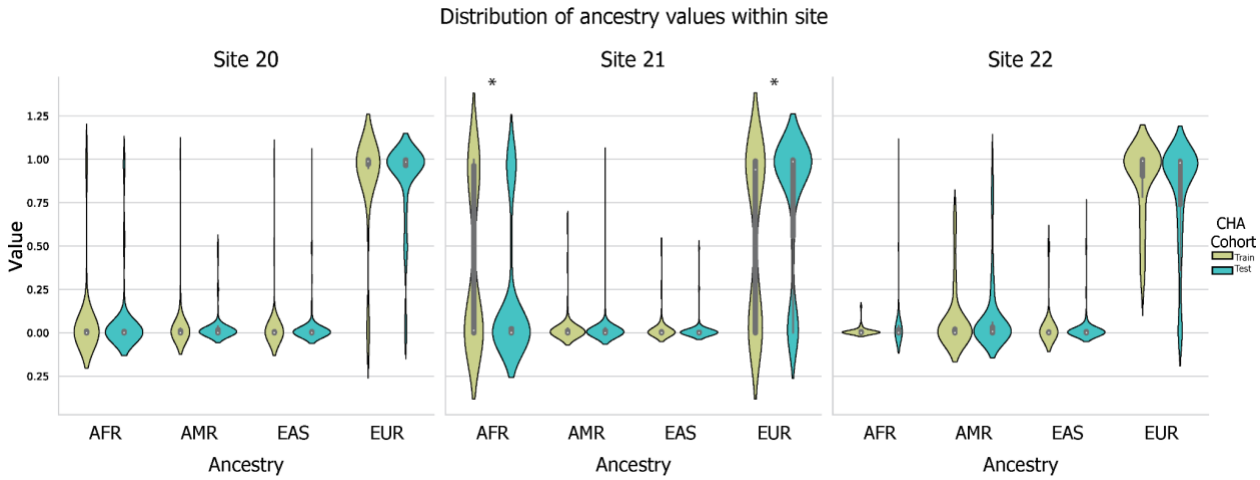

Figure S3: Participant genetic ancestry.

The three sites significantly differed in mean genetic ancestry. To respect this diversity and add generalizability to our heritability analyses, we selected CHA training subjects to reflect site sample demographics as best as possible. Shown here are the distributions of participants' scores for the participants allocated for CHA train or test cohorts. Significance of differences along each dimension between CHA cohorts were tested with a two-tailed independent samples t-test and * denotes $p < 0.05$ after Bonferroni correction.

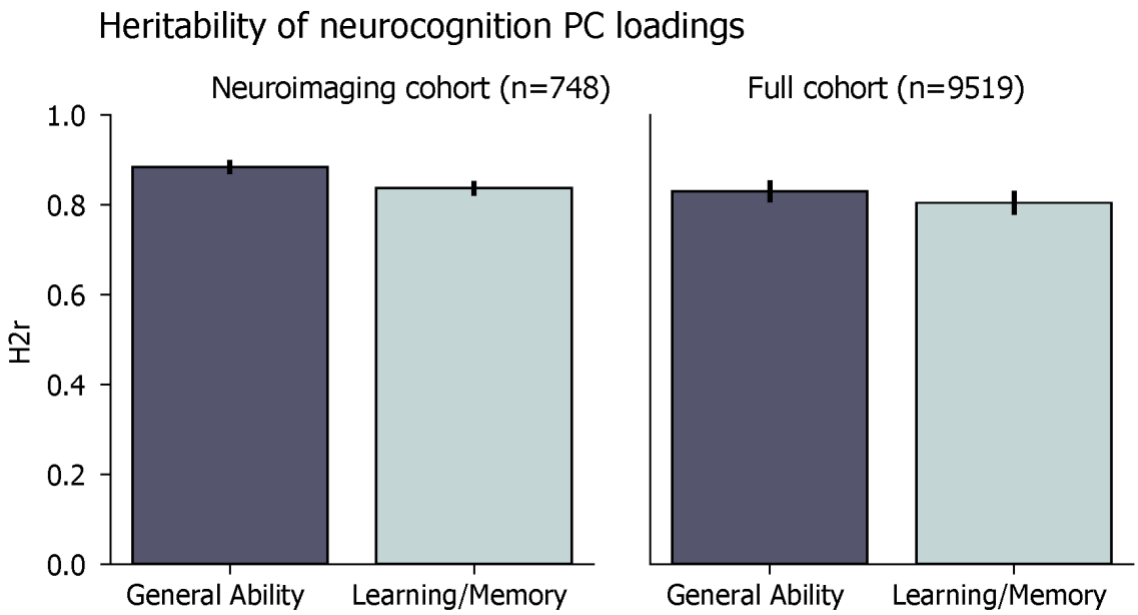

Figure S4: Heritability of neurocognition PC loadings

Heritability of neurocognition PC solution loadings for general cognitive ability and learning/memory.

Left: H2r of general cognitive ability and learning/memory were computed using SOLAR polygenic across participants in our twin cohort (full sample: n = 778; with complete data: n = 748). h^2 of general cognitive ability = 0.884 ± 0.01; h^2 of learning/memory = 0.837 ± 0.01 (reported as SOLAR polygenic h2r +/- standard error).

Right: To evaluate whether the behavioral heritability effect was due to sampling bias toward the subjects included in the neuroimaging analysis, we recalculated H2r of the same components using the full ABCD study sample (full sample: n = 11,875; with complete data n = 9,519). Estimate of general cognitive ability = 0.830 ± 0.02, learning/memory = 0.800 ± 0.02.

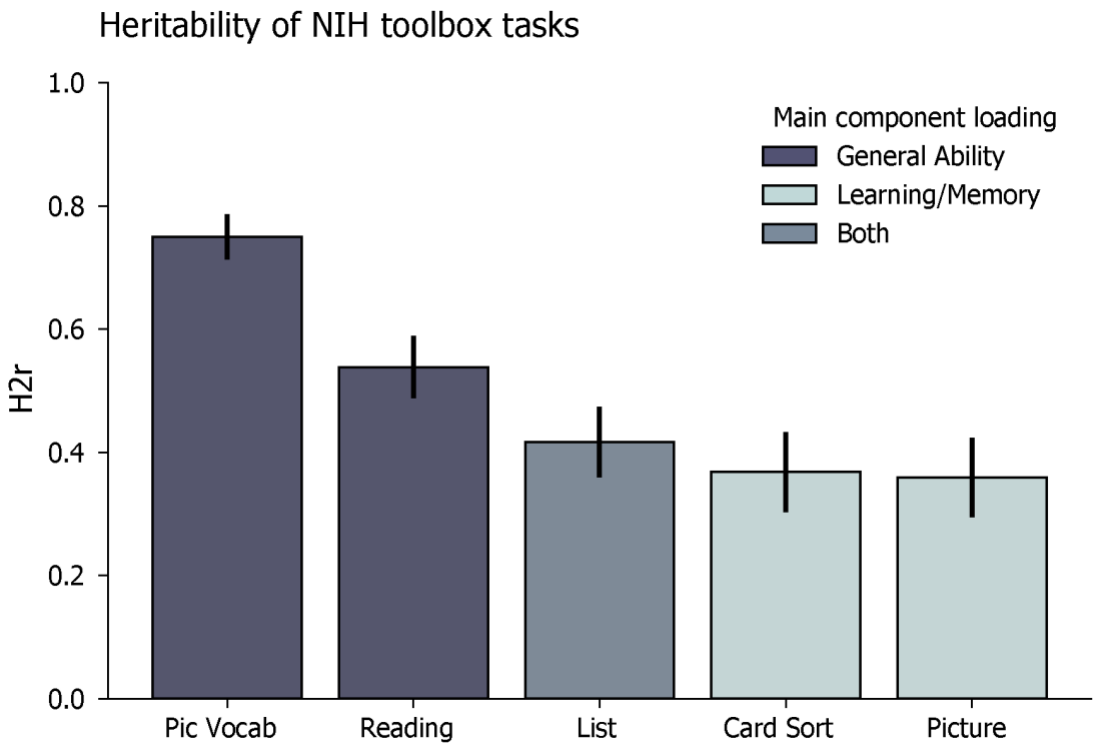

Figure S5: Heritability of individual tasks loading onto neurocognition PCs

Heritability analysis of the individual NIH Toolbox tasks loading onto the general cognitive ability and learning/memory components. Tasks loading more strongly onto the general cognitive ability component (*pic vocab, reading*) showed stronger heritability whereas tasks loading more strongly onto the learning/memory component (*card sort, picture*) showed weaker heritability and a task loading onto both components evenly (*list sorting*) showed intermediate heritability.

Abbreviation: PicVocab = Toolbox Picture Vocabulary Task (language skills and verbal intellect); Reading = Toolbox Oral Reading Recognition Task (read and pronounce single words), List = Toolbox List Sorting Working Memory Test; CardSort = Toolbox Dimensional Change Card Sort Task (cognitive flexibility); Picture = Toolbox Picture Sequence Memory Test.

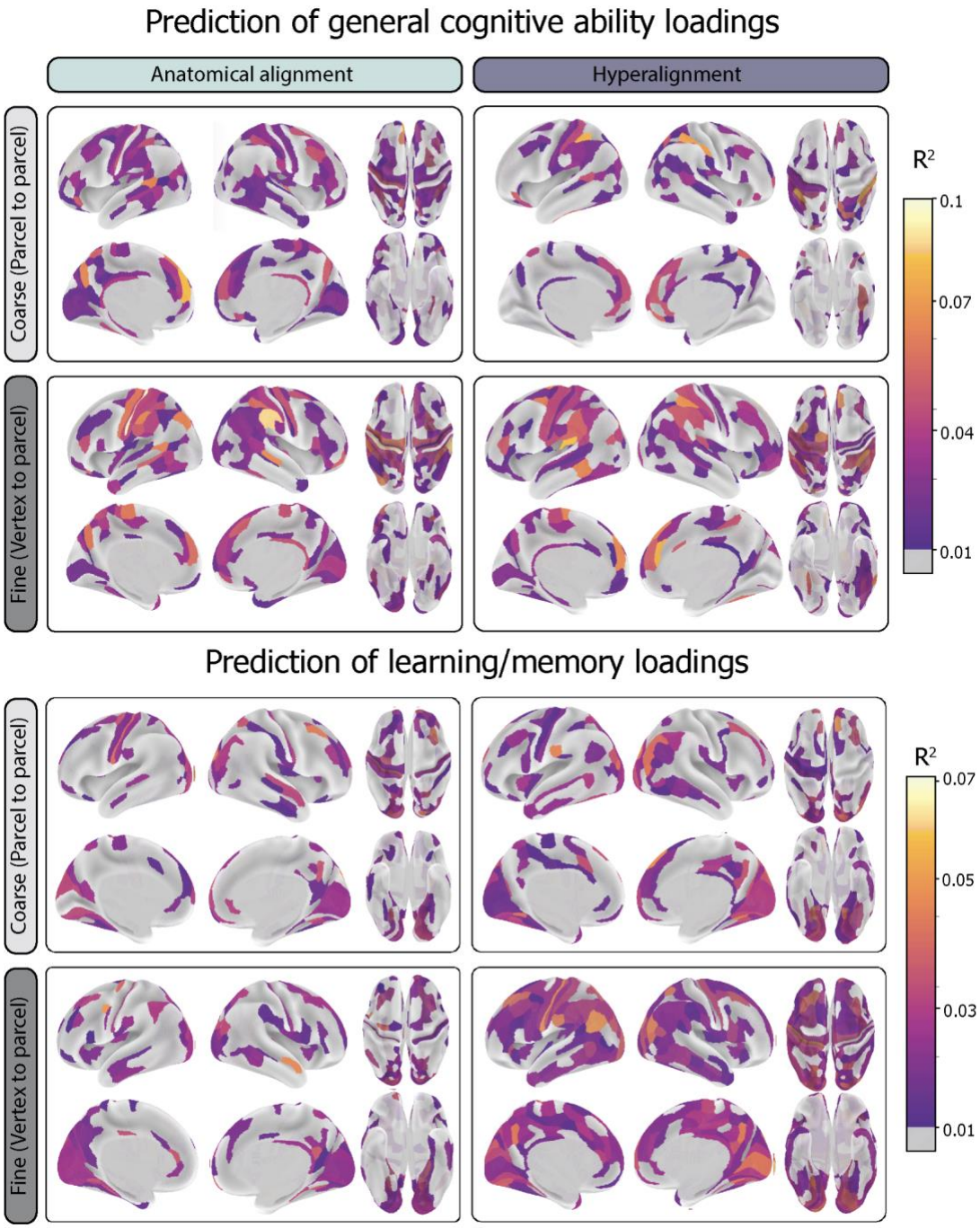

Figure S6: Prediction of neurocognition displayed on cortical surface.

Prediction of individual differences in the general cognitive ability component (top) and the learning/memory component (bottom). R^2 values displayed for each parcel and significance assessed with 1000 permutations. Nonsignificant R^2 values ($p > 0.01$) displayed in gray.

References

1. Jansen, A. G., Mous, S. E., White, T., Posthuma, D. & Polderman, T. J. What twin studies tell us about the heritability of brain development, morphology, and function: a review. *Neuropsychol. Rev.* **25**, 27–46 (2015).
2. Glahn, D. C. *et al.* Genetic control over the resting brain. *Proc. Natl. Acad. Sci. U. S. A.* **107**, 1223–1228 (2010).
3. Miranda-Dominguez, O. *et al.* Heritability of the human connectome: A connectotyping study. *Network Neuroscience* vol. 02 175–199 (2018).
4. Blokland, G. A. M., de Zubicaray, G. I., McMahon, K. L. & Wright, M. J. Genetic and Environmental Influences on Neuroimaging Phenotypes: A Meta-Analytical Perspective on Twin Imaging Studies. *Twin Res. Hum. Genet. Off. J. Int. Soc. Twin Stud.* **15**, 351–371 (2012).
5. Yang, Z. *et al.* Genetic and Environmental Contributions to Functional Connectivity Architecture of the Human Brain. *Cereb. Cortex N. Y. N 1991* **26**, 2341–2352 (2016).
6. Haxby, J. V., Guntupalli, J. S., Nastase, S. A. & Feilong, M. Hyperalignment: Modeling shared information encoded in idiosyncratic cortical topographies. *eLife* **9**,.
7. Haak, K. V., Marquand, A. F. & Beckmann, C. F. Connectopic mapping with resting-state fMRI. *NeuroImage* **170**, 83–94 (2018).
8. Lin, Q., Yoo, K., Shen, X., Constable, T. R. & Chun, M. M. Functional Connectivity during Encoding Predicts Individual Differences in Long-Term Memory. *J. Cogn. Neurosci.* **33**, 2279–2296 (2021).
9. Rosenberg, M. D. *et al.* A neuromarker of sustained attention from whole-brain functional connectivity. *Nat. Neurosci.* **19**, 165–171 (2016).

10. Finn, E. S. *et al.* Functional connectome fingerprinting: identifying individuals using patterns of brain connectivity. *Nat. Neurosci.* **18**, 1664–1671 (2015).
11. Sripada, C. *et al.* Prediction of neurocognition in youth from resting state fMRI. *Mol. Psychiatry* **25**, 3413–3421 (2020).
12. Feilong, M., Guntupalli, J. S. & Haxby, J. V. The neural basis of intelligence in fine-grained cortical topographies. *eLife* vol. 10 e64058 (2021).
13. Cui, Z. *et al.* Individual Variation in Functional Topography of Association Networks in Youth. *Neuron* vol. 106 340-353.e8 (2020).
14. Dosenbach, N. U. F. *et al.* Prediction of Individual Brain Maturity Using fMRI. *Science* **329**, 1358–1361 (2010).
15. Chen, J. *et al.* Shared and unique brain network features predict cognitive, personality, and mental health scores in the ABCD study. *Nat. Commun.* **13**, 2217 (2022).
16. Casey, B. J. *et al.* The Adolescent Brain Cognitive Development (ABCD) study: Imaging acquisition across 21 sites. *Dev Cogn Neurosci* vol. 32 43–54 (2018).
17. Iacono, W. G. *et al.* The utility of twins in developmental cognitive neuroscience research: How twins strengthen the ABCD research design. *Dev. Cogn. Neurosci.* **32**, 30–42 (2017).
18. Brouwer, R. M. *et al.* Heritability of brain volume change and its relation to intelligence. *NeuroImage* **100**, 676–683 (2014).
19. Elliott, L. T. *et al.* Genome-wide association studies of brain imaging phenotypes in UK Biobank. *Nature* **562**, 210–216 (2018).
20. Peper, J. S. *et al.* Heritability of regional and global brain structure at the onset of puberty: A magnetic resonance imaging study in 9-year-old twin pairs. *Hum. Brain Mapp.* **30**, 2184–2196 (2009).

21. Thompson, P. M. *et al.* Genetic influences on brain structure. *Nat. Neurosci.* **4**, 1253–1258 (2001).

22. Colclough, G. L. *et al.* The heritability of multi-modal connectivity in human brain activity. *eLife* vol. 6 e20178 (2017).

23. Barber, A. D., Hegarty, C. E., Lindquist, M. & Karlsgodt, K. H. Heritability of Functional Connectivity in Resting State: Assessment of the Dynamic Mean, Dynamic Variance, and Static Connectivity across Networks. *Cereb. Cortex N. Y. NY* **31**, 2834–2844 (2021).

24. Anderson, K. M. *et al.* Heritability of individualized cortical network topography. *Proc. Natl. Acad. Sci.* **118**, e2016271118 (2021).

25. Ge, T., Holmes, A. J., Buckner, R. L., Smoller, J. W. & Sabuncu, M. R. Heritability analysis with repeat measurements and its application to resting-state functional connectivity. *Proc. Natl. Acad. Sci.* **114**, 5521–5526 (2017).

26. Fu, Y. *et al.* Genetic influences on resting-state functional networks: A twin study. *Hum. Brain Mapp.* **36**, 3959–3972 (2015).

27. Schmitt, J. E. *et al.* The dynamic role of genetics on cortical patterning during childhood and adolescence. *Proc. Natl. Acad. Sci.* **111**, 6774–6779 (2014).

28. Lenroot, R. K. *et al.* Differences in genetic and environmental influences on the human cerebral cortex associated with development during childhood and adolescence. *Hum. Brain Mapp.* **30**, 163–174 (2009).

29. Kennedy, J. T. *et al.* Reliability and stability challenges in ABCD task fMRI data. *NeuroImage* **252**, 119046 (2022).

30. Achterberg, M. *et al.* Distinctive heritability patterns of subcortical-prefrontal cortex resting state connectivity in childhood: A twin study. *NeuroImage* **175**, 138–149 (2018).

31. Marek, S. *et al.* Reproducible brain-wide association studies require thousands of individuals. *Nature* **603**, 654–660 (2022).

32. Bandettini, P. A. *et al.* The challenge of BWAs: Unknown unknowns in feature space and variance. *Med* (2022).

33. Glasser, M. F. *et al.* A multi-modal parcellation of human cerebral cortex. *Nature* vol. 536 171–178 (2016).

34. Kong, R. *et al.* Spatial Topography of Individual-Specific Cortical Networks Predicts Human Cognition, Personality, and Emotion. *Cereb. Cortex* **29**, 2533–2551 (2019).

35. Kong, R. *et al.* Individual-Specific Areal-Level Parcellations Improve Functional Connectivity Prediction of Behavior. *Cereb. Cortex* **31**, 4477–4500 (2021).

36. Haxby, J. V. *et al.* A Common, High-Dimensional Model of the Representational Space in Human Ventral Temporal Cortex. *Neuron* **72**, 404–416 (2011).

37. Guntupalli, J. S. *et al.* A Model of Representational Spaces in Human Cortex. *Cereb. Cortex* **26**, 2919–2934 (2016).

38. Guntupalli, J. S., Feilong, M. & Haxby, J. V. A computational model of shared fine-scale structure in the human connectome. *PLOS Comput. Biol.* **14**, e1006120 (2018).

39. Nastase, S. A., Liu, Y.-F., Hillman, H., Norman, K. A. & Hasson, U. Leveraging shared connectivity to aggregate heterogeneous datasets into a common response space. *NeuroImage* **217**, 116865 (2020).

40. Busch, E. L. *et al.* Hybrid hyperalignment: A single high-dimensional model of shared information embedded in cortical patterns of response and functional connectivity. *NeuroImage* **233**, 117975 (2021).

41. Feilong, M., Nastase, S. A., Guntupalli, J. S. & Haxby, J. V. Reliable individual differences

in fine-grained cortical functional architecture. *NeuroImage* **183**, 375–386 (2018).

42. Paus, T., Keshavan, M. & Giedd, J. N. Why do many psychiatric disorders emerge during adolescence? *Nat. Rev. Neurosci.* **9**, 947–957 (2008).
43. Power, J. D., Barnes, K. A., Snyder, A. Z., Schlaggar, B. L. & Petersen, S. E. Spurious but systematic correlations in functional connectivity MRI networks arise from subject motion. *NeuroImage* **59**, 2142–2154 (2012).
44. Van Dijk, K. R. A., Sabuncu, M. R. & Buckner, R. L. The influence of head motion on intrinsic functional connectivity MRI. *NeuroImage* **59**, 431–438 (2012).
45. Noble, S. *et al.* Influences on the Test–Retest Reliability of Functional Connectivity MRI and its Relationship with Behavioral Utility. *Cereb. Cortex* **27**, 5415–5429 (2017).
46. Plomin, R. & Deary, I. J. Genetics and intelligence differences: five special findings. *Mol. Psychiatry* **20**, 98–108 (2015).
47. Bouchard, T. J. Genetic Influence on Human Psychological Traits: A Survey. *Curr. Dir. Psychol. Sci.* **13**, 148–151 (2004).
48. Mollon, J. *et al.* Genetic influence on cognitive development between childhood and adulthood. *Mol. Psychiatry* **26**, 656–665 (2021).
49. Plomin, R. & Spinath, F. M. Intelligence: Genetics, Genes, and Genomics. *J. Pers. Soc. Psychol.* **86**, 112 (20040112).
50. Fletcher, J. M., Marks, A. D. G., Hine, D. W. & Coventry, W. L. Heritability of Preferred Thinking Styles and a Genetic Link to Working Memory Capacity. *Twin Res. Hum. Genet.* **17**, 526–534 (2014).
51. Thompson, W. K. *et al.* The structure of cognition in 9 and 10 year-old children and associations with problem behaviors: Findings from the ABCD study's baseline

neurocognitive battery. *Developmental Cognitive Neuroscience* vol. 36 100606 (2019).

52. Marek, S. *et al.* Identifying reproducible individual differences in childhood functional brain networks: An ABCD study. *Dev. Cogn. Neurosci.* **40**, (2019).
53. Johnson, M. H. Interactive Specialization: A domain-general framework for human functional brain development? *Dev. Cogn. Neurosci.* **1**, 7–21 (2011).
54. Rosenberg, M. D. *et al.* Behavioral and Neural Signatures of Working Memory in Childhood. *J. Neurosci.* **40**, 5090–5104 (2020).
55. DeYoung, C. G. *et al.* Reproducible between-person brain-behavior associations do not always require thousands of individuals. Preprint at https://doi.org/10.31234/osf.io/sfnmk (2022).
56. Dubois, J. & Adolphs, R. Building a Science of Individual Differences from fMRI. *Trends Cogn Sci* vol. 20 425–443 (2016).
57. Dubois, J., Galdi, P., Paul, L. K. & Adolphs, R. A distributed brain network predicts general intelligence from resting-state human neuroimaging data. *Philos. Trans. R. Soc. B Biol. Sci.* **373**, 20170284 (2018).
58. Greene, A. S., Gao, S., Scheinost, D. & Constable, R. T. Task-induced brain state manipulation improves prediction of individual traits. *Nat. Commun.* **9**, 2807 (2018).
59. Satterthwaite, T. D. *et al.* Impact of in-scanner head motion on multiple measures of functional connectivity: Relevance for studies of neurodevelopment in youth. *NeuroImage* **60**, 623–632 (2012).
60. Need, A. C. & Goldstein, D. B. Next generation disparities in human genomics: concerns and remedies. *Trends Genet.* **25**, 489–494 (2009).
61. Savage, J. E. *et al.* Genome-wide association meta-analysis in 269,867 individuals identifies

new genetic and functional links to intelligence. *Nat. Genet.* **50**, 912–919 (2018).

62. Popejoy, A. B. & Fullerton, S. M. Genomics is failing on diversity. *Nature* **538**, 161–164 (2016).
63. Grasby, K. L. *et al.* The genetic architecture of the human cerebral cortex. *Science* **367**, eaay6690 (2020).
64. Haworth, C. M. A. *et al.* The heritability of general cognitive ability increases linearly from childhood to young adulthood. *Mol. Psychiatry* **15**, 1112–1120 (2010).
65. Hagler, D. J. *et al.* Image processing and analysis methods for the Adolescent Brain Cognitive Development Study. *NeuroImage* **202**, 116091 (2019).
66. Dosenbach, N. U. *et al.* Real-time motion analytics during brain MRI improve data quality and reduce costs. *Neuroimage* **161**, 80–93 (2017).
67. Feczko, E. *et al.* Adolescent Brain Cognitive Development (ABCD) Community MRI Collection and Utilities. 2021.07.09.451638 Preprint at https://doi.org/10.1101/2021.07.09.451638 (2021).
68. Gorgolewski, K. J. *et al.* The brain imaging data structure, a format for organizing and describing outputs of neuroimaging experiments. *Sci. Data* **3**, 160044 (2016).
69. dcm2bids. (2022).
70. Li, X., Morgan, P. S., Ashburner, J., Smith, J. & Rorden, C. The first step for neuroimaging data analysis: DICOM to NIfTI conversion. *J. Neurosci. Methods* **264**, 47–56 (2016).
71. dsturge, Earl, E. & kathy-snider. DCAN-Labs/abcd-hcp-pipeline: release v0.0.0. (2019) doi:10.5281/zenodo.2587210.
72. Glasser, M. F. *et al.* The minimal preprocessing pipelines for the Human Connectome Project. *NeuroImage* **80**, 105–124 (2013).

73. Dale, A. M., Fischl, B. & Sereno, M. I. Cortical surface-based analysis. I. Segmentation and surface reconstruction. *NeuroImage* **9**, 179–194 (1999).

74. Fischl, B. FreeSurfer. *NeuroImage* **62**, 774–781 (2012).

75. Avants, B. B. *et al.* A reproducible evaluation of ANTs similarity metric performance in brain image registration. *NeuroImage* **54**, 2033–2044 (2011).

76. dcan signal processing. (2022).

77. Fair, D. A. *et al.* Correction of respiratory artifacts in MRI head motion estimates. *NeuroImage* **208**, 116400 (2020).

78. Birn, R. M. *et al.* The effect of scan length on the reliability of resting-state fMRI connectivity estimates. *NeuroImage* **83**, 550–558 (2013).

79. Fair, D. *et al.* Distinct neural signatures detected for ADHD subtypes after controlling for micro-movements in resting state functional connectivity MRI data. *Front. Syst. Neurosci.* **6**, (2013).

80. Mantel, N. Ranking Procedures for Arbitrarily Restricted Observation. *Biometrics* **23**, 65–78 (1967).

81. Carr, J. mantel. (2021).

82. Almasy, L. & Blangero, J. Multipoint quantitative-trait linkage analysis in general pedigrees. *Am. J. Hum. Genet.* **62**, 1198–1211 (1998).

83. Falconer, D. S. *Introduction to quantitative genetics*. (Pearson Education India, 1996).